Accelerated corrosion investigations on mechanical hybrid rockbolt steel

by F.D. Agrensa[1], J. Hadjigeorgiou[1], S.J. Thorpe[1]

Affiliation:
[1] University of Toronto, Toronto, Ontario, Canada

Correspondence to:
J. Hadjigeorgiou

Email:
john.hadjigeorgiou@utoronto.ca

Dates:
Received: 09 Dec. 2025
Revised: .13 Jul. 2026
Accepted: 28 Jul. 2026
Published: Aug. 2026

How to cite:
Agrensa, F.D., Hadjigeorgiou, J., Thorpe, S.J. 2026. Accelerated corrosion investigations on mechanical hybrid rockbolt steel. *Journal of the Southern African Institute of Mining and Metallurgy*, vol. 126, no. 8, pp. 491 – 502

DOI ID:
https://doi.org/10.17159/2411-9717/3868/2026

ORCiD:
F.D. Agrensa
https://orcid.org/0009-0007-1625-2308
J. Hadjigeorgiou
https://orcid.org/0000-0002-6047-3964
S.J. Thorpe
https://orcid.org/0000-0001-8263-2498

Abstract

The recent introduction in underground mines of mechanical hybrid rockbolts has been driven by efforts to eliminate the use of resin in heavily fractured ground. Mechanical hybrid rockbolts consists of a steel tendon mechanically anchored within a friction unit. Installation of mechanical hybrid rockbolts is percussion-driven by the rock drill and the mechanical anchor is subsequently activated using rotation. The bolt configuration and installation process overcome issues associated with hole closures and the use of resin.

Recent work has focused on understanding the behaviour of the rockbolts under quasi-static and dynamic conditions but there is scant information on the anticipated performance in corrosive underground environments. This paper reports the results of a comprehensive accelerated corrosion investigation of the principal components of mechanical hybrid rockbolt. This can aid in establishing the long-term suitability of mechanical hybrid rockbolt in corrosive environments.

Keywords

Mechanical hybrid rockbolts (MHR), steel tendon and friction unit, steel properties, accelerated corrosion, long-term performance

Introduction

The selection of rock reinforcement for underground excavations in rock requires matching the anticipated capacity and deformation for the anticipated loads. To achieve the design capacity of a particular rockbolt is the ability for it to be installed under adverse conditions such as highly stressed, friable, and fractured ground. An additional challenge is ensuring the long-term performance of installed ground support elements over time. Corrosion is one of the contributing factors that can result in degradation and possible failure of a rock reinforcement element.

In highly stressed, friable, and fractured rock the effectiveness of resin-grouted rockbolts can be limited. This is associated with resin migration into joints that can result in gaps or voids along the rockbolt bar, not attaining the full column and partially mixed resin grout penetrating the rock mass. Another concern is that borehole closures can prevent the installation of resin cartridges. These scenarios can result in a poorly installed resin grouted rockbolt not reaching its design capacity.

Mechanical hybrid rockbolts (MHR) are a relatively recent addition to rock reinforcement options for difficult installation conditions. MHR employs a specifically designed mechanical point anchor bolt installed inside a friction rock stabiliser. Limited tests at Mount Charlotte suggested that the configuration of a specially designed mechanical anchor installed in a friction rock stabiliser provided good static capacity (Carlton et al., 2013). Andrews (2019) reported that MHR have been successfully implemented in highly stressed and fractured rock mass conditions at mine sites in Australia and South Africa.

There are two fundamental concerns for the widespread application of MHR. The first is the absence of supporting quantifiable data on the performance of the mechanical friction bolts under a range of loading conditions and their potential susceptibility to corrosion making them not a good option for long term applications in corrosive environments.

Recent work by Knox and Hadjigeorgiou (2024a) provided the first significant data on the load displacement behaviour of MHR under different loading configurations ranging from 0^0 (axial load) to 30^0 (a combination of axial and shear with the axial load being dominant), to 60^0 (where the shear component becomes dominant over the axial load), and pure shear (90^0).

There is surprisingly more information on the behaviour of different MHR under impact testing using the continuous tube configuration, as reported by Darlington et al. (2019), Vallati et al. (2022), Evans (2022), and more recently by Knox and Hadjigeorgiou (2024b). The justification for the use of the continuous tube configuration is based on the design and energy dissipation function of the rockbolt. The tendon anchored within the friction unit of an MHR is assumed to be loaded independently, consequently, the direct loading of the tendons is justifiable.

This paper aims to address a knowledge gap specific to the susceptibility to corrosion of MHR. A deep and high stress underground mine was exploring the use of MHR in areas that were potentially susceptible to corrosion. As part of a comprehensive investigation of new products, the mine investigated the susceptibility to corrosion of two commercially available MHRs, the MD rockbolt (Sandvik, 2025) and the Vulcan rockbolt (Epiroc, 2025).

As illustrated in Figure 1, both MHR employ a solid bar/rebar inside a friction unit with an anchor near or at the distal end. The mechanical dynamic (MD) bolt head comprises a ring welded onto the friction unit, a nut, and another ring attached to the rebar. This allows both the friction unit and the rebar to directly sustain any axial load induced by the movement of the rock mass. In the Vulcan bolt, the plate is attached to the bar connected through the spherical seat, the load indicator, and the nut. Consequently, the bar will predominantly sustain an induced axial load due to a rock mass movement near the bolt head. In both cases, the reinforcement mechanism can only be achieved if the anchor is successfully activated.

In the absence of long-term exposure data, there is a significant knowledge gap on the susceptibility to corrosion of MHR. Determining the susceptibility of rockbolts to corrosion of ground support requires a knowledge of the steel properties, rockbolt configuration, and the exposure time and severity of the environment. This investigation focused on the steel properties of the main components of the rockbolts in a succession of accelerated corrosion experiments. The influence of the chemical composition and the steel microstructures was also discussed.

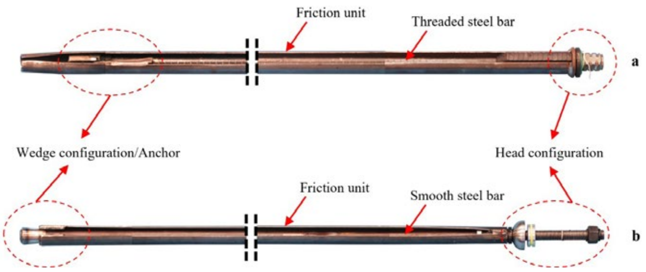

Figure 1—Configuration of two MHR: a. MD bolt b. Vulcan bolt

Figure 2—MHR installation using a twin boom drill rig, (Knox, Hadjigeorgiou, 2024b)

Installation considerations

MHR can be installed using a range of equipment including platform bolters, specialised bolters, and twin boom drill rigs, as per Figure 2. The MHR used in this investigation employs similar installation procedures, illustrated in Figure 3.

A borehole is drilled with a bit diameter smaller than the outer diameter of the friction unit component. The rockbolt, with a faceplate attached, is then driven into the borehole through the percussive force of the bolter. After the rockbolt is fully inserted, a torque is applied to the nut on the bolt head. Consequently, the anchor is pulled toward the bolt head, leading to an expansion of the wedge. The wedge expansion can reach up to 52 mm for the MD bolt, while the anchor of the Vulcan bolt with a 39 mm friction unit diameter can be expanded to approximately 43 mm in diameter. When the anchor is successfully activated, tension stress is induced along the rebar/bar component. As a result, an immediate reinforcing action is exerted on the rock mass.

Susceptibility to corrosion

The majority of rockbolts installed at underground mines are manufactured using low-carbon steels containing a variety of alloying elements. The chemical composition of steel controls its strength, hardenability, formability, weldability, ductility, and susceptibility to corrosion. In practice, multiple combinations of

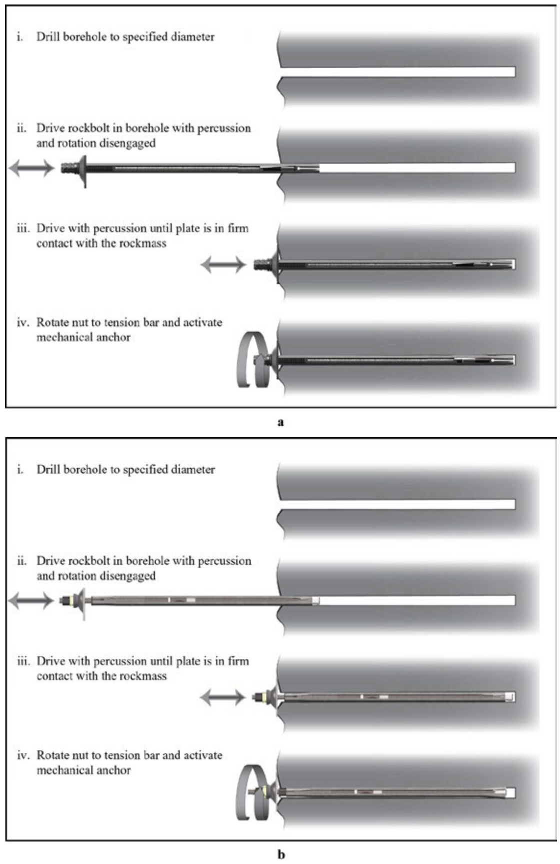

Figure 3—Installation steps for: a. MD bolt b. Vulcan bolt (Knox, Hadjigeorgiou, 2023)

alloying elements can be used to meet the mechanical performance requirements of steel and rockbolts.

In underground mining environments, rockbolts are exposed to a range of corrosive environments. Atmospheric corrosion is controlled by factors such as temperature, relative humidity, airflow, and the presence of pollutants (Hadjigeorgiou et al., 2008). As the water vapour condenses onto the rockbolt, it triggers an electrochemical reaction. Aqueous corrosion occurs due to exposure to underground mine water. Rockbolts exposed to an aqueous environment are generally more susceptible to corrosion than those undergoing atmospheric corrosion.

Along with the water temperature, various parameters that indicate the presence of chemical species exacerbating the corrosion rate can be used to characterise the environment, such as pH, conductivity, total dissolved solids (TDS), the dissolved oxygen (DO) level, and concentration of aggressive anions (Cl^-, SO_4^{-2}, etc.). In addition, microorganisms present in the water can facilitate or inhibit the corrosion of rockbolts (Craig et al., 2016; Dorion, Hadjigeorgiou, 2020).The pH measures the concentration of H^+-ions in the solution, which also indicates the acidity/alkalinity of the solution. A solution with a higher concentration of H^+ will lead to a lower pH level. The dissolved oxygen (DO) is a measure of oxygen, a strong oxidising agent in the solution. The rate of mass transfer for chemical species is temperature-dependent. As the corrosion reaction involves an electron transfer step, the rate of electricity passing through a solution (conductivity) can also be an indicator. The total dissolved solid (TDS) measures the concentration of the dissolved substance in the solution. As the previously mentioned parameters increase, the corrosivity of the environment will consequently increase, resulting in an elevated corrosion rate. The influence of aggressive anions, e.g., Cl^- and SO_4^{-2}, affect not only the general corrosion rate but are also associated with localised forms of attack such as pitting corrosion. Since pitting corrosion rates may be orders of magnitude greater than general corrosion rates, the latter may not be a representative indicator for long-term bolt integrity. The lowered rate is due to the decreased solubility of oxygen in the presence of the dissolved NaCl. A significant mass loss occurring at the pit will negatively affect the structural integrity of the metal by acting as a point of stress concentration and crack nucleation.

The susceptibility of any rockbolt to corrosion is a complex process influenced by multiple parameters, including the corrosive environment, the rockbolt configuration, and the material properties. The corrosion rate of rockbolt steel depends on various factors when the rockbolts are exposed to an aqueous corrosive environment. The influencing factors can be generally divided into two: the corrosivity of the aqueous environment or the solution and the corrosion resistance of the steel. The corrosivity of the aqueous environment, or the external factors to the rockbolt material, is associated with the presence of chemical species and microbacteria or temperatures that affect the kinetics behaviour of the corrosion reaction. The corrosion resistance of the steel material is attributed to the presence of a protective coating, the alloying elements, and the resultant microstructure upon fabrication.

Dorion and Hadjigeorgiou (2014) provided a high-level comparison between ground support elements and their susceptibility to corrosion. Although these guidelines are used at mine sites to select appropriate rockbolts in a range of corrosive environments it is limited in that it does not include MHR. Given the short history of MHR there are no empirical data at this time to assess their corrosion susceptibility. This is of concern given that they employ a two-component system (friction unit and rebar/rod) that, in the absence of a resin, is likely to be susceptible to corrosion. This may limit the application of mechanical hybrid rockbolts to relatively short-term applications in corrosive environments, thus, the driving force for ongoing work at the University of Toronto on the long-term performance of MHR in corrosive environments. The present work reports on the results of a research programme focused on the influence of the chemical composition and the resultant steel microstructure of the main components of MHR using accelerated corrosion experiments.

Experimental investigations

The objective of this investigation was to provide a first set of data on the potential corrosion susceptibility of the recently developed MHR. To this end, two MHR from different suppliers have been subjected to a series of electrochemical tests. Of interest is that mechanical hybrid rockbolts comprise two distinct main components, the rebar/rod and the friction unit, which use different

Table 1

Chemical composition of steels for MHR (in weight%)

Element		**C (%)**	**Mn (%)**	**P (%)**	**S (%)**	**Si (%)**	**Cu (%)**	**Ni (%)**	**Cr (%)**
MHR #1	Tendon/bar	0.229	1.44	0.024	0.025	0.59	0.02	0.01	0.04
	Friction unit	0.188	0.83	0.025	0.021	0.34	0.02	0.01	0.03
MHR #2	Tendon/bar	0.230	1.46	0.013	0.004	0.62	0.10	0.07	0.10
	Friction unit	0.091	1.14	0.008	0.003	0.20	0.01	0.01	0.02
Element		V (%)	Mo (%)	Al (%)	Co (%)	Ti (%)	Pb (%)	Nb (%)	Fe (%)
MHR #1	Tendon/bar	0.05	<0.01	<0.01	<0.01	<0.01	<0.01	0.01	Balance
	Friction unit	0.02	<0.01	<0.01	0.01	<0.01	<0.01	0.02	Balance
MHR #2	Tendon/bar	0.07	0.02	<0.01	<0.01	<0.01	<0.01	0.01	Balance
	Friction unit	<0.01	<0.01	0.04	<0.01	0.02	<0.01	0.03	Balance

steels. The concern was whether there was significant variation between the corrosion behaviour of the two components and between different products.

Although both commercially available rockbolt types are also available with a protective galvanisation coating, this investigation aimed to quantify the anticipated corrosion rate of the core steel when exposed to an aggressive environment. This investigation established the chemical composition of the different steel components, the resulting material hardness, and the susceptibility of the employed steel components to corrosion when exposed to an aggressive environment. The paper reports the results of these investigations with reference to MHR #1 and MHR #2.

Chemical composition of the mechanical hybrid rockbolts

The chemical composition of steel for each rockbolt component was determined through inductively coupled plasma atomic emission spectroscopy/optical emission spectroscopy (ICP-AES/ICP-OES) and carbon and sulphur analysis as per ASTM E1479-16 and ASTM E1019-11, respectively. The chemical composition of each component is summarised in Table 1. The reported value is the average value out of three samples. The variance among samples prepared from the same component of a specific rockbolt tested was negligible.

A comparison of the chemical composition between the bar and friction unit steels indicates that the bar/tendon component has a higher concentration of C, Mn, Si, Cr, and V than the friction unit component on the same MHR product. This is reasonable as the bar component is the primary component of the rockbolt that is expected to sustain most of the imposed load. Furthermore, these elements are associated with increased strength through either precipitation of carbides, or interstitial and substitutional solid solution hardening.

From a corrosion perspective, the corrosion resistance of the bar steel of MHR #2 was expected to be lower than that of the friction unit component due to a higher difference in the mass fraction of C and P. However, this should be ameliorated with higher Si and Cr contents. Based on the S content, MHR #2 has the cleanest steel chemistry. The presence of S will increase the probability of MnS inclusion formation, adversely affecting the mechanical and corrosion resistance. MHR #1 also has an appreciably higher P content, potentially leading to poor corrosion performance. There is no significant difference in the mass fraction of the elements associated with enhancing the protective nature of the oxide layer among the rockbolts.

Material hardness of steel for MHR

To investigate the mechanical properties of steel materials for MHR, Rockwell hardness B tests were performed in accordance with ASTM E18-22. The HRBW value was determined by measuring the depth of indentation induced by pushing a 1.588 mm tungsten carbide ball indenter at 100 kgf of total test force into the steel sample. Prior to the test, the surface of the steel sample was ground by using 1200-grit SiC paper. Conversion from HRBW to the approximate tensile strength was made based on the conversion table provided by ISO 18265:2013. Minimum tensile strength values suggested by ASTM F432-19 and ASTM A1011/A1011M-23 were determined for comparison purposes. It should be noted that the difference in the minimum tensile strength is attributed to the different components and steel grades specified by suppliers.

All steel materials complied with the requirements stated in the ASTM (Table 2). In both MHR, the rebar/bar steel has a higher hardness than the friction unit steel on the same product. Moreover, the difference in the hardness of both bars was significant, while the friction unit of both products had similar hardness.

Steel microstructure

In addition to the chemical composition of the steel, understanding the microstructural constituents in an MHR can help interpret the corrosion performance by focusing on the role of grain size, stable phases and their volume fraction, grain boundaries, etc. Based on this information, the specific role of some alloying elements can be further investigated, particularly in terms of their association with the variation in corrosion performance. While the final microstructure is fundamentally a function of the chemical composition of steel and the heat treatment, the discussion is focused on the stable phases and their effects on the corrosion resistance of steel.

To obtain the microstructural information of each component from both MHR products, a sample was first prepared by sectioning the main component of the rockbolt. The sample surface was then progressively ground using 400-, 600-, and 1200-grit SiC paper before being subjected to a 2-step polishing process. In this stage, a mirror-like surface was obtained using two consecutive polishing steps with 3 μm and 1 μm diamond paste. The microstructure was revealed by etching the surface with Nital (2.5 vol% HNO_3 in ethanol). Scanning electron microscopy (SEM/EDX) was used for imaging and phase identification (Hitachi SU3500).

Figure 4 summarises the micrographs of each sample. In general, the bar and the friction unit of the MHR #1 and the bar for the MHR #2 were identified as a mixture of pearlite and primary alpha ferrite, where the α-ferrite is the matrix phase. The steel for MHR #2 friction unit has the least amount of pearlitic phase in its ferrite matrix. A trace of inclusions was also seen on both mechanical hybrid rockbolt samples, and these were more

Table 2

Rockwell B hardness and approximate tensile strength of steel material for MHR

Hardness test	MHR #1		MHR #2	
	Bar	Friction unit	Bar	Friction unit
Rockwell B Hardness (HRBW)	92.3 ± 1.5	90.4 ± 0.2	95.9 ± 0.6	90.3 ± 0.3
Approximate tensile strength (ISO 18265:2013)	655 ± 24 MPa	624 ± 4 MPa	721 ± 14 MPa	622 ± 4 MPa
Minimum tensile strength (ASTM F432-19 and ASTM A1011/A1011M-23)	620 MPa	480 MPa	690 MPa	480 MPa

apparent on the MHR #1 components. Image analysis using ImageJ software was performed on three micrographs of each steel sample to quantify the volume fraction of the pearlite phase and inclusions. Comparison of the volume fraction of these microconstituents among steel samples is summarised in Table 3. In general, the steel for the bar component has a higher pearlitic volume fraction than the friction unit steel on the same MHR sample, consistent with the higher carbon content as reported in Table 1. A significantly higher volume fraction of inclusions was identified on the friction unit steel of the MHR #1.

The electrochemical properties of microconstituents and the associated volume fraction present in the steel will influence the susceptibility to corrosion. Variations in the corrosion rate of carbon steel as a function of various microstructures were reported by Clover et al. (2005), where an increased corrosion resistance of predominantly very fine ferrite microstructure was observed compared to a banded ferrite-pearlite microstructure. Cementite (Fe_3C) in an acidic chloride solution is more noble and corrosion-resistant than ferrite (Kadowaki et al., 2019). When the cementite and ferrite are coupled and exposed to a corrosive solution, galvanic corrosion will occur, accelerating the corrosion rate as the cementite will serve as a cathodic site. Although the cementite in pearlitic steel is inert due to the galvanic coupling, preferential corrosion of the ferrite-cementite interface will eventually cause the ejection of the cementite phase (Hayden et al., 2022). As a consequence, more steel surfaces will be exposed to the solution. Similar effects of sulphide inclusion, e.g., MnS, on the overall corrosion performance of steel can also be interpreted since the inclusion is more noble than the Fe matrix (Janik-Czachor et al., 1972).

Based on the image analysis results (Table 3), the steel for MHR #1 (bar and friction unit) and MHR #2 bar were expected to have a relatively higher corrosion rate. The high-volume fraction of the pearlite phase is indicative of a high amount of cementite due to the lamellar structure of pearlite. This will enable galvanic corrosion, leading to an elevated corrosion rate. The corrosion resistance of the friction unit steel for MHR #1 is further exacerbated by the comparatively higher fraction of inclusions.

Table 3

Volume fractions of pearlitic phase and inclusion on steel for MHR based on image analysis

	Component	$V_{pearlite}$ (%)	$V_{inclusion}$ (%)
MHR #1	Bar	34.14 ± 6.55	0.07 ± 0.05
	Friction unit	20.64 ± 6.03	0.28 ± 0.03
MHR #2	Bar	37.24 ± 1.56	0.02 ± 0.01
	Friction unit	0.85 ± 0.65	0.07 ± 0.02

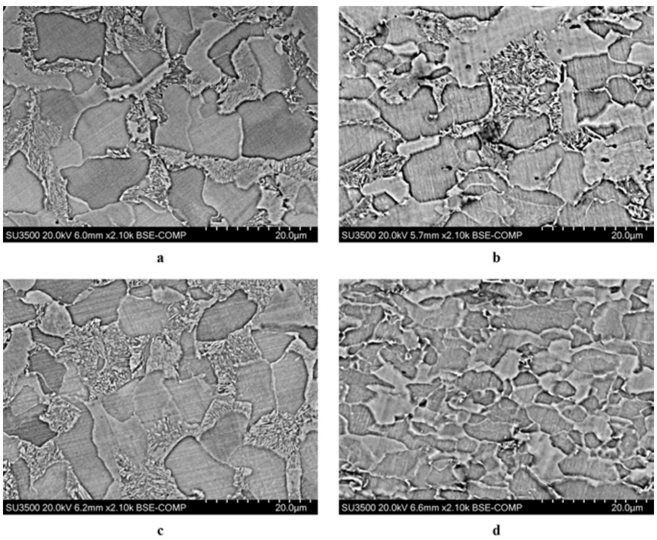

Figure 4—Microstructures of steels for: a. Bar of MHR #1 b. Friction unit of MHR #1 c. Bar of MHR #2 d. Friction Unit of MHR #2

Accelerated corrosion testing

In the absence of long-term data on the susceptibility to corrosion of the new generation of MHR, accelerated corrosion tests can provide some preliminary insight into their behaviour. Accelerated corrosion tests have been used in the past to highlight variations in the performance of expandable rockbolts (Hadjigeorgiou et al., 2020), friction rock stabilisers (Hadjigeorgiou et al., 2023), and welded mesh and straps (Hadjigeorgiou et al., 2024). These results demonstrated that the chemical composition of the steel chosen by a given supplier could have a significant impact on corrosion performance when exposed to aggressive environments. Given that MHR do not employ resin it is reasonable to anticipate that they would also be susceptible to corrosion.

Investigating electrochemical properties associated with the corrosion reaction of rockbolt steel can assist in characterising the in situ corrosion performance in a specific corrosive environment. The electrochemical properties are obtained from a plurality of accelerated corrosion tests, of which the results are considered indicative of the actual corrosion performance. Nevertheless, accelerated corrosion testing can provide fundamental corrosion properties that are useful in various phases of the ground support design process, especially when corrosion is one of the concerns. Moreover, accelerated corrosion testing is generally faster than the conventional immersion testing of the ground support elements.

Accelerated corrosion tests on steel materials used for MHR were performed to characterise the corrosion performance of each rockbolt steel. For the MHR, the experiment focuses on the main components, the steel tendon and the friction unit, as both components play essential roles in establishing the reinforcement

Table 4

Chemical composition of the synthetic mine water as the lixiviate for the accelerated corrosion test (Hadjigeorgiou et al., 2020)

Chemical compound	Formula	g/L
Chemical compound	Formula	g/L
Magnesium sulphate heptahydrate	$MgSO_4.7H_2O$	31.44
Calcium sulphate dihydrate	$CaSO_4.2H_2O$	1.76
Ferrous sulphate heptahydrate	$FeSO_4.7H_2O$	1.24
Aluminum sulphate octa decahydrate	$Al_2(SO_4)_3.18H_2O$	10.49
Zinc sulphate heptahydrate	$ZnSO_4.7H_2O$	3.87
Sodium sulphate anhydrite	Na_2SO_4	0.12
Sodium chloride	NaCl	0.41

action of the rockbolt. The non-galvanised (black) rockbolts were obtained from different suppliers. The same lixiviate, or synthetic mine water used in Hadjigeorgiou et al. (2020), Hadjigeorgiou et al. (2023), and Hadjigeorgiou et al. (2024) was employed as the electrolyte in the experiment. It was prepared by dissolving chemical compounds (salts) listed in Table 4 in de-ionised (DI) water. The final pH of the lixiviate was adjusted to 2.7 using diluted sulphuric acid (H_2SO_4). Based on the low pH and high concentration of aqueous chemical species, the lixiviate represents an aggressive mine environment.

Electrochemical techniques for accelerated corrosion test and analysis

Each rockbolt steel sample was subjected to accelerated corrosion tests comprising three (3) electrochemical techniques: open-circuit potential (OCP), linear polarisation resistance (LPR), and potentiodynamic polarisation. The sequence, potential window, and scan rate for the electrochemical techniques are provided in Figure 5. During the OCP measurement, no current was allowed to pass between the counter and working electrodes and the potential was measured as a function of time until the steel was equilibrated with the electrolyte. This is followed by the LPR technique, following the procedure outlined in ASTM G59 – 97 using the conditions noted in Figure 5. With a small potential window about the E_{OCP}, the LPR is considered a non-destructive technique, thus allowing further techniques to be performed in sequence for the investigation. Lastly, the potentiodynamic anodic polarisation technique was carried out by adapting the procedure in ASTM G5 – 14, as noted in Figure 5.

Polarisation resistance (R_p) resulting from the LPR measurement will be used to determine the corrosion current density by using the equation proposed by Stern and Geary (1957):

$$i_{corr} = \frac{\beta_a \beta_c}{2.303\, R_p(\beta_a + \beta_c)} \quad [1]$$

where; βa: anodic Tafel slope; β_c: cathodic Tafel slope; R_p: polarisation resistance; i_{corr}: corrosion current density. By using Faraday's law, the corrosion rate (r), in mm/year, can be calculated from the corrosion current density (i_{corr}) (Dean Jr. et al., 1971):

$$r = 0.00327\, \frac{i_{corr}}{\rho}\, EW \quad [2]$$

where; ρ: density of sample; *EW*: equivalent weight. The equivalent weight, which is perceived as the mass of metal/alloy in grams that will be oxidised as a result of one Faraday (96,489 C) electric charge, is calculated in accordance with ASTM G102 – 89.

Sample preparation and experimental set-up

For the accelerated corrosion test, three (3) replicates were prepared from the steel material of each sample/rockbolt component to ensure the repeatability of the result. The procedure for preparing the replicates is summarised in Figure 6. Generally, the preparation involves soldering a Cu-wire to the replicate and grinding the surface of interest to a 600-grit final surface using SiC paper. Due to the small size of the bar replicate and irregular edges resulting from sectioning, an epoxy resin encapsulation is used to protect against localised corrosion/pitting. Moreover, the order of soldering and grinding to the 600-grit final surface of the bar component also differs from that of the friction unit component. The last step of the replicate preparation is masking the area of interest using Amercoat 90HSTM epoxy with three (3) coating layers. Once the coating had been fully cured, a high-resolution optical image was taken, and the area of the surface was determined by using ImageJ software.

The experimental setup for the accelerated corrosion test is shown in Figure 7. A three-electrode setup similar to that of Hadjigeorgiou et al. (2020), Hadjigeorgiou et al. (2023), and Hadjigeorgiou et al. (2024) was applied in this work. A three-electrode cell consisting of a working, counter, and reference electrode was used. The working electrode is the replicate of the rockbolt steel, while the counter electrode is a fine platinum mesh. An Ag/AgCl electrode filled with 3M KCl was used as the reference electrode that was calibrated before each test. Each test was carried out in a minimum of 500 ml lixiviate and purged with Argon gas at around 150 ml/min for 60 minutes to ensure complete deaeration before the electrochemical techniques were initiated. The temperature of the lixiviate is kept at 30oC during the purging and the accelerated corrosion test using a water bath.

Corrosion morphology and electrochemical properties of rockbolt steel

Based on the electrochemical techniques employed, electrochemical properties obtained include the open-circuit potential (E_{OCP}),

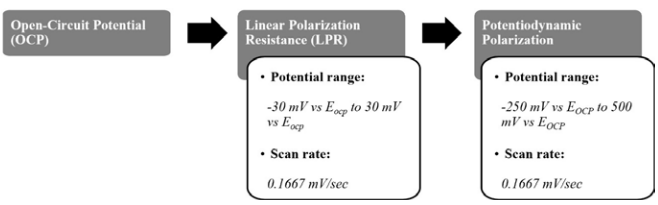

Figure 5—Sequences, the potential range of applied bias, and scan rate for electrochemical techniques for accelerated corrosion test

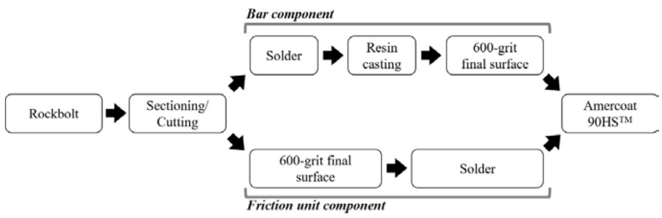

Figure 6—Schematic diagram of the procedure to prepare replicates for the accelerated corrosion test

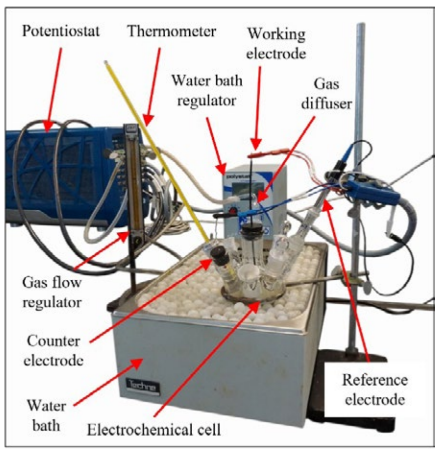

Figure 7—Experimental setup for the accelerated corrosion test

polarisation resistance (R_p), Tafel slopes, corrosion potential (E_{corr}), and corrosion current density ($i_{corr\ PP}$). Measured potentials are converted to the saturated calomel electrode (SCE) scale. Further analysis was performed to determine the corrosion rate from linear polarisation resistance (LPR) and potentiodynamic polarisation results. A high-resolution optical image was taken right after the acceleration corrosion test to examine the surface condition of every replicate.

Corrosion morphology

A comparison of the sample surface before and after the accelerated corrosion tests is summarised in Figures 8 and 9. Based on visual observations, the corrosion morphology of all samples was relatively uniform. The morphology is characterised as general corrosion with the formation of an oxide layer. Pitting or crevice corrosion was not found on the sample surface.

Open-circuit potential (OCP) measurements

In the OCP test, the working electrode is unbiased and equilibrates with the solution over time. The open-circuit potential was measured after the working electrode had equilibrated for 60 minutes. The open-circuit potentials for all samples range from -0.673 V to -0.648 V vs SCE (-0.432 V to -0.407 V vs SHE). In this electrochemical system, based on the open-circuit potential of which the magnitude is situated between the most feasible oxidation and reduction reactions (Bard et al., 2022), the corrosion reactions on all rockbolt samples involved the dissolution of iron as the anodic reaction (E_{red}^{o} = -0.44 V vs SHE) and the hydrogen evolution reaction as the cathodic reaction (E_{red}^{o} = 0.00 V vs SHE).

The measurement of open-circuit potential for all samples over the first 60 minutes of immersion is shown in Figure 10. The MHR #1 bar/tendon steel is the most active steel with the lowest open-circuit potential. In contrast, the friction unit steel of the MHR #2 has the most noble open-circuit potential. The difference in the open-circuit potential between those two steel materials is 35 mV. It is also interesting to note that the steel used for both bar components is more active than the steel used for both friction unit components of the MHR. A comparison between the components of both products shows that the steel material for MHR #1 is more active than that of MHR #2.

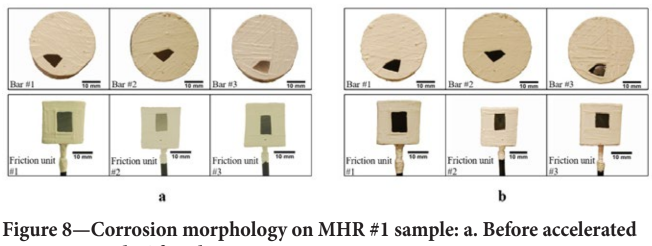

Figure 8—Corrosion morphology on MHR #1 sample: a. Before accelerated corrosion test b. After the test

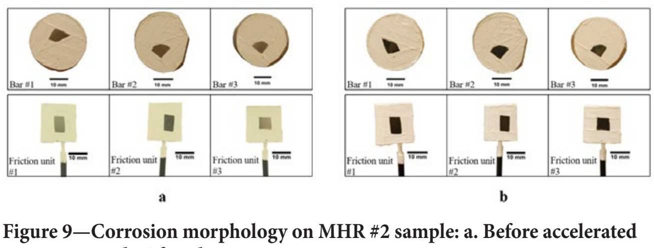

Figure 9—Corrosion morphology on MHR #2 sample: a. Before accelerated corrosion test b. After the test

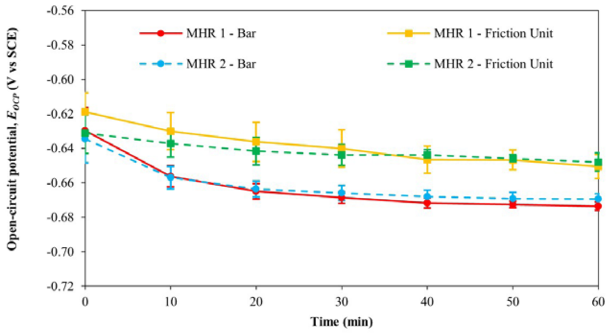

Figure 10—Open-circuit potential measurements of steels from two MHRs

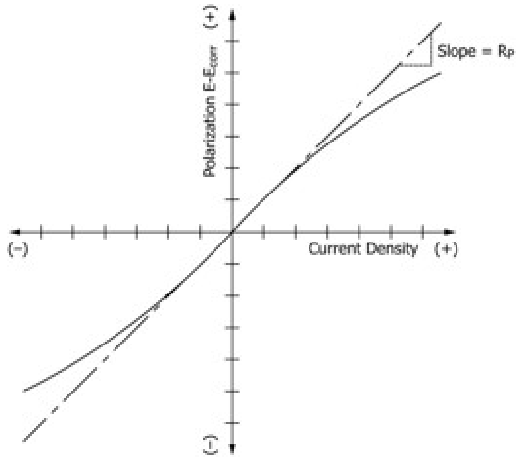

Figure 11—Hypothetical linear polarisation plot and measurement of polarisation (ASTM G3 – 14)

Linear Polarization Resistance (LPR)

The polarization resistance was measured as the slope of the potential–current density behaviour of the sample within an apparent linear region about the origin (Figure 11). The polarization plot was established by applying a small cathodic and anodic bias (± 30 mV) about the open-circuit potential at a constant sweep rate while recording the current density response of the working electrode. As the polarization resistance is inversely proportional to the corrosion rate, the more current generated due to a small magnitude of polarisation, the higher the corrosion rate of the metal/alloy will be. The linear polarisation plot resulting from the LPR measurement of all rockbolt samples is shown in Figures 12 and 13.

The corrosion rate of rockbolt samples estimated from the LPR results is summarised in Table 5. The results in Figure 12 and Figure 13 illustrate three separate runs on each of the rockbolt specimens and demonstrate good reproducibility between samples. It should be noted that the corrosion rate calculation requires Tafel slopes to be measured during the potentiodynamic polarisation test. Based on the LPR measurement, the corrosion rate of the bar components of both MHR is statistically equivalent. The corrosion rate of the MHR #1 is substantially greater than for the friction unit of MHR #2. For the MHR #1, the friction unit had a higher corrosion rate compared to the bar, while the reverse trend was observed in MHR #2. Overall, the steel for the friction unit component of MHR #1 has the highest corrosion rate for all the materials tested by LPR, and the lowest corrosion rate was observed for the friction unit of MHR #2.

Anodic potentiodynamic polarisation (AP)

In the potentiodynamic polarisation technique, the current response of the rockbolt sample was recorded as the electrode potential was polarised both cathodically and anodically. The magnitude of the applied voltage is significantly higher than that of the LPR technique, and the measurement is initiated by a cathodic polarisation followed by an anodic polarisation. A hypothetical potential-current density behaviour of metal, along with the interpretation of electrochemical properties resulting from the potentiodynamic polarisation technique, is shown in Figure 14. The corrosion current density and the corrosion potential are determined by the intersection of the extended Tafel behaviour observed at a relatively higher overpotential. The slopes of these two linear regimes defined as the anodic Tafel slope (βa) and cathodic Tafel slope (βc), which characterise the kinetics of the metal dissolution reaction and the hydrogen evolution reaction, respectively.

The polarisation plots recorded in the potentiodynamic technique for rockbolt samples are presented in Figures 16 and 17. The plots indicate a good reproducibility of the potential - current behaviour among steel replicates of the same bolt component. Compared to the hypothetical polarisation plot in Figure 14, the polarisation plots of the rockbolt steel are all unsymmetrical about the corrosion potential as the axis of symmetry. This indicates that within the potential window applied for the potentiodynamic polarisation technique, the redox reactions and the rate of reactions occurring at a higher anodic and cathodic overpotential are not the same. The cathodic current is produced from the hydrogen evolution reaction, whereas the anodic current is most likely associated with the Fe dissolving into Fe^{2+}.

The results of potentiodynamic polarisation measurements are presented in Table 6. The variance of results among replicates of the same rockbolt component is statistically negligible. Regarding the corrosion potential, the steel for the MHR #1 bar is the most active, while the most noble steel is of the friction unit for the MHR #2. Using this electrochemical technique, the corrosion rate of the bar of MHR #1 is greater than MHR #2. Similarly, the corrosion rate for the friction unit of MHR #1 is greater than that of the friction unit of MHR #2. The highest corrosion rate was observed on the steel for the MHR #1 friction unit. It is interesting to note that the estimated corrosion rates of the friction unit steels are slightly higher than the bar steels on the same product. A very high cathodic Tafel slope, which was also observed in Hadjigeorgiou et al.

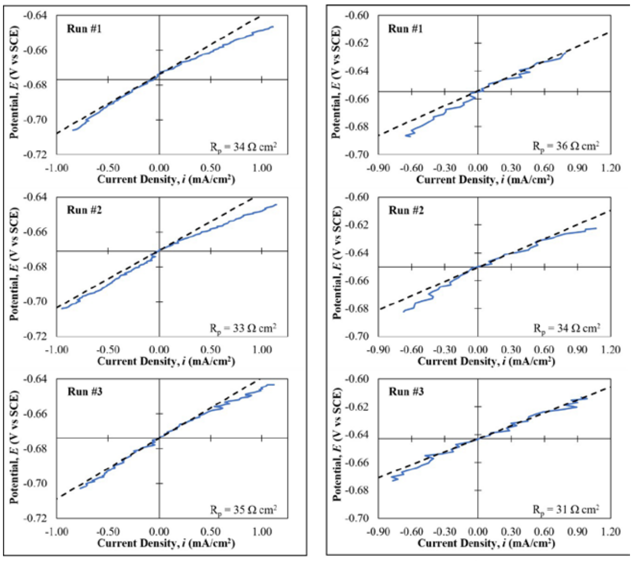

a b

Figure 12—Linear polarisation resistance results for MHR #1: a. Bar steel b. Friction unit steel

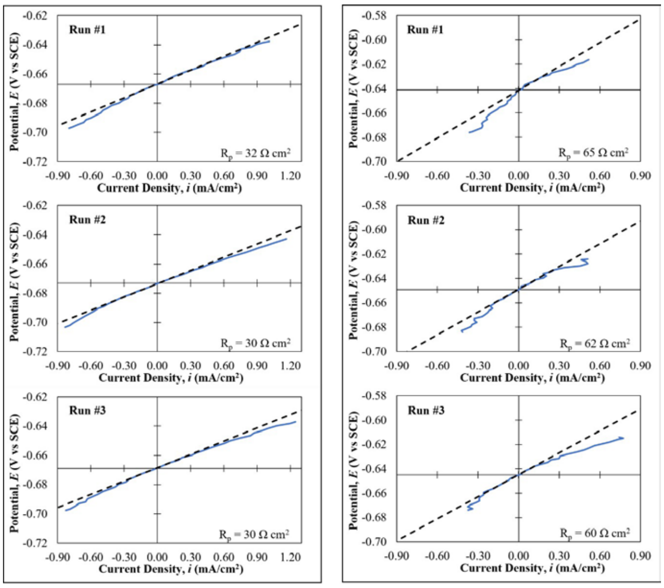

a b

Figure 13—Linear polarisation resistance results of MHR #2: a. Bar steel b. Friction unit steel

Table 5

Summary of results and analyses of LPR measurement for all rockbolt samples

Rockbolt	Component	Rp (Ω cm²)	$i_{corr,Rp}$ (mA cm⁻²)	r_{Rp} (mm yr⁻¹)
MHR #1	Bar	34.0 ± 1.0	0.95 ± 0.04	11.12 ± 0.48
	Friction unit	33.7 ± 2.5	1.21 ± 0.08	14.24 ± 0.92
MHR #2	Bar	30.7 ± 1.2	1.03 ± 0.03	12.08 ± 0.31
	Friction unit	62.3 ± 2.5	0.56 ± 0.02	6.56 ± 0.27

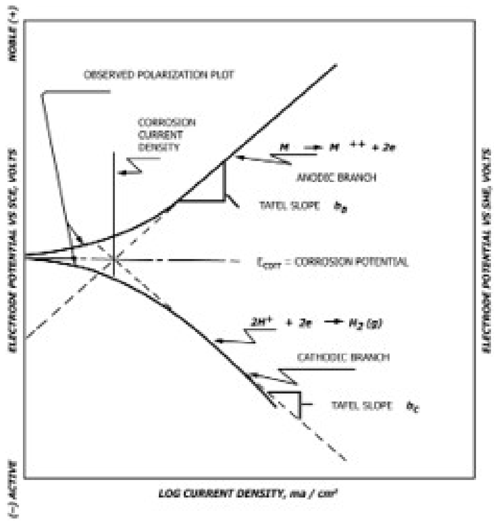

Figure 14—Hypothetical cathodic and anodic Tafel polarisation plot (ASTM G3 - 14)

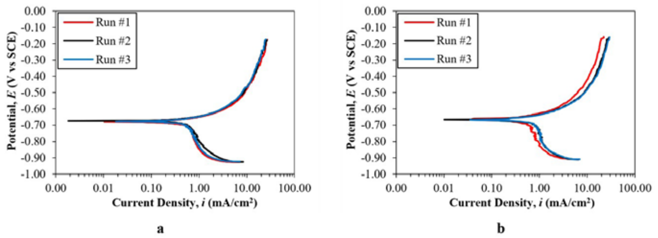

Figure 15—Potentiodynamic polarisation plot for MHR #1: a. Bar b. Friction unit

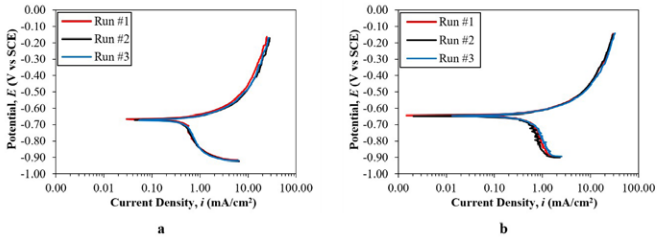

Figure 16—Potentiodynamic polarisation plot for MHR #2: a. Bar b. Friction unit

(2020), Hadjigeorgiou et al. (2023), and Hadjigeorgiou et al. (2024a, 2024b) was measured in this experiment. The high cathodic Tafel slope is a characteristic of a mixed electrochemical mechanism on the electrode surface and indicates that the cathodic reaction is not purely a hydrogen evolution reaction (HER).

Discussion

The potential and corrosion rates resulting from the accelerated corrosion test are summarised in Table 7. The open-circuit potential of the same rockbolt sample agrees well with the corrosion potential measured during potentiodynamic polarisation measurements. The slight variance in both open-circuit and corrosion potential indicates that all rockbolt steels are similar in thermodynamic behaviour.

Comparing the corrosion rate obtained from LPR and potentiodynamic measurements for the bar components, LPR measurements showed a similar trend in corrosion rate, with the exception of the bar component of MHR #2. A slightly higher corrosion rate was statistically measured for all of the LPR measurements compared to AP measurements. The corrosion rate from AP may appear lower because they are more influenced by factors such as the formation of passive or barrier type films and the rate of accumulation of metal ions near the surface because of the higher anodic potentials reached during the test. The corrosion rate of the friction unit steel for MHR #1 was substantially higher than all other components, regardless of the technique employed.

The extent of variation in the electrochemical properties in Table 7 is most likely attributable to the variation in the exact chemical composition of each rockbolt steel. By using mixed potential theory to explain the variation in the open-circuit potential and the corrosion potential, the most active (lowest) potential of the MHR #1 bar steel can be associated with the highest total mass fraction of alloying elements that are more active than Fe such as Mn and Si. The presence of alloying elements such as C, S, Cu, Ni, Mo, Co, and P from atomic or microscale perspectives can potentially lead to more noble open-circuit or corrosion potentials. However, quantifying how these elements influence the E_{OCP} and E_{CORR} is complex. This is due to the formation of the chemical compounds, i.e., carbides and sulphide inclusions, that also play essential roles in the magnitude of the potentials, not only due to the presence of substitutional alloying elements. The same case was encountered while investigating the relationship between the chemical compositions and the corrosion rate. Nevertheless, the magnitude of the corrosion rate may be attributed to two electrochemical mechanisms. The first is the formation of stable, protective oxide film, most likely contributed by Si, Cu, Ni, Cr, Mo, Al, Co, Ti, and Nb. The underlying assumption for this mechanism is that one or more of these elements are partitioned into or stabilise the resultant oxide film; thus, the corrosion rate is reduced. The second is micro-galvanic corrosion due to chemical compounds formed by C and S, leading to an elevated corrosion rate.

When carbon is added to the steel within the hypoeutectoid composition, where the heat treatment process only involves heating the steel to the upper critical temperature and then cooling it at a slow rate to room temperature, a large portion of the C content will react with Fe to form cementite and is precipitated in the form of pearlite. Comparing the corrosion rate based on the

Table 6

Summary of electrochemical properties of steel samples obtained from the potentiodynamic polarisation measurements

Rockbolt	Component	E_{corr} (V vs SCE)	$i_{corr,PP}$ (mA cm^{-2})	r_{PP} (mm yr^{-1})	βa (mV dec^{-1})	βc (mV dec^{-1})
MHR #1	Bar	-0.678 ± 0.003	0.533 ± 0.023	6.26 ± 0.27	86 ± 4	516 ± 20
	Friction unit	-0.665 ± 0.003	0.653 ± 0.098	7.72 ± 1.16	115 ± 4	488 ± 7
MHR #2	Bar	-0.668 ± 0.003	0.458 ± 0.014	5.40 ± 0.17	82 ± 2	598 ± 2
	Friction unit	-0.645 ± 0.001	0.473 ± 0.042	5.53 ± 0.49	96 ± 1	490 ± 4

Table 7

Comparison of potentials and corrosion rates estimated from different electrochemical techniques

Rockbolt	Component	E_{OCP} (V vs SCE)	E_{corr} (V vs SCE)	r_{Rp} (mm yr^{-1})	r_{PP} (mm yr^{-1})
MHR #1	Bar	-0.673 ± 0.002	-0.678 ± 0.003	11.12 ± 0.48	6.26 ± 0.27
	Friction unit	-0.651 ± 0.007	-0.665 ± 0.003	14.24 ± 0.92	7.72 ± 1.16
MHR #2	Bar	-0.669 ± 0.003	-0.668 ± 0.003	12.08 ± 0.31	5.40 ± 0.17
	Friction unit	-0.648 ± 0.005	-0.645 ± 0.001	6.56 ± 0.27	5.53 ± 0.49

LPR technique and the volume fraction of pearlite shows that the steel with a high pearlite volume fraction (bar and friction unit of MHR #1 and bar of MHR #2) has a higher corrosion rate (r_{LPR}). With the micro-galvanic coupling between the pearlite and ferrite phases, where the carbide phase acts as a cathodic site, the anodic dissolution of the boundary between both phases and/or the ferrite phase is accelerated, leading to a higher corrosion rate. An interesting condition was seen on the friction unit steel of MHR #1, indicating a significant influence of the presence of inclusions on the corrosion performance. Even though the steel does not have the highest volume fraction of the pearlite phase, the highest corrosion rate is most likely attributed to the significantly high-volume fraction of inclusions.

The long-term behaviour of MHR may be affected by the overall and relative corrosion rates of their various components. On MHR #1, the corrosion rate of the steel for the bar is slightly lower than that of the friction unit. The opposite condition is identified on MHR # 2 in LPR tests. The comparison also shows that the corrosion rates of the bar components from different suppliers are similar. This may indicate that the reduction of the ultimate capacity of the bar between both MHR will not differ significantly. On the other hand, a significant variation in the corrosion rate between the friction unit components is observed. For an MHR product of which the friction unit will also sustain a relatively greater portion of the axial load, a significant loss in the cross-sectional area in extreme conditions may also lead to a loss of capacity. A heavily corroded friction unit will negatively impact the anchoring performance of the bolt to achieve its designed ultimate capacity.

Conclusion

Mechanical hybrid rockbolts are a relatively recent addition to the reinforcement toolbox to support underground excavations in rock. A major impetus for their use is that the installation process improves the rockbolt resilience to hole closures and avoids issues associated with the use of resin. Recent experimental data, as reported in Carlton et al. (2013) and Knox and Hadjigeorgiou (2024), demonstrated that the higher yielding capacity of MHR would also make them suitable for squeezing and rock burst prone conditions.

A potential limitation of MHR is their long-term performance in corrosive environments. Currently there are no empirical data capturing the long-term performance of MHR in corrosive environments. This is a major shortcoming to assess the consequences of using MHR. This paper is part of a multi-year research project on MHR aiming to quantify their mechanical behaviour and susceptibility to corrosion. This involves mechanical quasi-static and impact tests, accelerated corrosion tests, long-term laboratory immersion tests, and field trials in a selected mine site.

An investigation of the corrosion performance of the steel used in two types of MHR has been conducted to understand the corrosion resistance between rockbolt components and the variability among the two products. Accelerated corrosion techniques, where each component is uniformly exposed to the same corrosive synthetic mine water, revealed that each MHR had different corrosion resistance.

Overall MHR #2 performed better than MHR #1 in this phase of the investigation that included material testing and accelerated corrosion. The results are more instructive when considering separately the performance of the rebar/bar steel the friction unit steel.

In both MHR, the rebar/bar steel had a higher hardness than the friction unit steel on the same product. This is attributed to the higher concentration of C, Mn, Si, Cr, and V than the friction unit component for the same MHR product. These elements are associated with increased strength through either precipitation of carbides, or interstitial and substitutional solid solution hardening. A significant variation, however, was observed between the tensile strength of the bar for MHR #2 (721 ± 14 MPa) and MHR #1 (655 ± 24 MPa).

MHR #1 is more susceptible to corrosion compared to MHR #2. Although the steel bar from both products has similar corrosion resistance, a significant variation was observed in the friction unit components.

The corrosion rate using linear polarisation resistance and potentiodynamic polarisation measurements for the friction unit steel for MHR #1 was substantially higher than that observed for MHR #2. This was explained by the chemical composition of the steel. A contributing factor to the higher corrosion rate for the friction unit steel of MHR #1, is the significantly high-volume fraction of inclusion determined by image analysis of SEM images of the rockbolt steel (based on ASTM E1245-03).

For an MHR of which the friction unit will also sustain a relatively greater portion of the axial load, a significant loss in the cross-sectional area in extreme conditions may also lead to a loss of capacity. A heavily corroded friction unit will negatively impact the anchoring performance of the bolt to achieve its designed ultimate capacity. This is consistent with previous work by Dorion and Hadjigeorgiou (2014), whereby the residual capacity of friction rock stabilisers was shown to be a function of the design capacity and the corrosion rate.

A further practical implication is that there can be significant variation in the corrosion resistance between different MHR products. This underscores the need to establish strict criteria on corrosion performance of these new MHRs. This can have significant implications in selecting a particular MHR for long-term applications.

Acknowledgements

The authors would like to acknowledge the financial support of Vale Base Metals and the Natural Science and Engineering Research Council of Canada. The authors would also like to acknowledge the collaboration from Sandvik and Epiroc who provided the rockbolt samples used in these investigations.

References

Andrews, P. 2019. Ground support selection rationale: a Gold Fields perspective. Australian Centre for Geomechanics. 15–28 p.

ASTM A1011/A1011M-23. 2023. Standard Specification for Steel, Sheet and Strip, Hot-Rolled, Carbon, Structural, High-Strength Low-Alloy, High-Strength Low-Alloy with Improved Formability, and Ultra-High Strength. West Conshohocken (PA): ASTM International, 100 Barr Harbor Drive, PO Box C700, West Conshohocken, PA 19428-2959. US.

ASTM E1245-03. 2023. Standard Practice for Determining the Inclusion or Second-Phase Constituent Content of Metals by Automatic Image Analysis. West Conshohocken (PA): ASTM International, 100 Barr Harbor Drive, PO Box C700, West Conshohocken, PA 19428-2959. US.

ASTM E18-22. 2022. Standard test methods for Rockwell hardness of metallic materials. West Conshohocken (PA): ASTM International, 100 Barr Harbor Drive, PO Box C700, West Conshohocken, PA 19428-2959. US.

ASTM E1019-11. 2011. Standard Test Methods for Determination of Carbon, Sulfur, Nitrogen, and Oxygen in Steel, Iron, Nickel, and Cobalt Alloys by Various Combustion and Fusion Techniques. West Conshohocken (PA): ASTM International, 100 Barr Harbor Drive, PO Box C700, West Conshohocken, PA 19428-2959. US.

ASTM E1479-16. 2016. Standard Practice for Describing and Specifying Inductively Coupled Plasma Atomic Emission Spectrometers. West Conshohocken (PA): ASTM International, 100 Barr Harbor Drive, PO Box C700, West Conshohocken, PA 19428-2959. US.

ASTM F432-19. 2019. Standard Specification for Roof and Rock Bolts and Accessories.

ASTM G3 - 14. 2019. Standard Practice for Conventions Applicable to Electrochemical Measurements in Corrosion Testing. West Conshohocken (PA): ASTM International, 100 Barr Harbor Drive, PO Box C700, West Conshohocken, PA 19428-2959. US.

ASTM G5 - 14. 2021. Standard Reference Test Method for Making Potentiodynamic Anodic Polarization Measurements. West Conshohocken (PA): ASTM International, 100 Barr Harbor Drive, PO Box C700, West Conshohocken, PA 19428-2959. US.

ASTM G59 - 97. 2020. Standard Test Method for Conducting Potentiodynamic Polarization Resistance Measurements. West Conshohocken (PA): ASTM International, 100 Barr Harbor Drive, PO Box C700, West Conshohocken, PA 19428-2959. US.

ASTM G102 - 89. 2015. Standard Practice for Calculation of Corrosion Rates and Related Information from Electrochemical Measurements. West Conshohocken (PA): ASTM International, 100 Barr Harbor Drive, PO Box C700, West Conshohocken, PA 19428-2959. US.

Bard, A.J., Faulkner, L.R., White, H.S. 2022. Electrochemical Methods Fundamentals and Applications. 3rd ed. John Wiley & Sons, Ltd: Hoboken, NJ.

Carlton, R., Darlington, B., Mikula, P. 2013. In situ dynamic drop testing of the MD bolt at Mt Charlotte Gold Mine. Australian Centre for Geomechanics. pp. 207–219.

Clover, D., Kinsella, B., Pejcic, B., De Marco, R. 2005. The Influence of Microstructure on the Corrosion Rate of Various Carbon Steels. Journal of Applied Electrochemistry vol. 35 (no. 2): pp. 139–149.

Craig, P., Serkan, S., Hagan, P., Hebblewhite, B., Vandermaat, A., Crosky, A., Elias, E. 2016. Investigations into the corrosive environments contributing to premature failure of Australian coal mine rock bolts. *International Journal of Mining Science and Technology* vol. 26, no. 1: pp. 59–64.

Darlington, B., Rataj, M., Roach, W. 2019. A new method to evaluate dynamic bolts and the development of a new dynamic rock bolt. *The Southern Africa Institute of Mining and Metallurgy*. Proceedings of the Ninth International Conference on Deep and High Stress Mining 2019: pp. 205–216.

Dean Jr., S.W., France Jr., W.D., Ketcham, S.J. 1971. Electrochemical methods. In W.H. Ailor (ed.), *Handbook on Corrosion Testing and Evaluation*, pp. 173–174. New York.

Dorion, J.F., Hadjigeorgiou, J. 2014. Corrosion considerations in the design and operation of rock support systems. *Mining Technology* vol. 123, no. 2, pp. 59–68.

Dorion, J.F., Hadjigeorgiou, J. 2020. Microbiologically Influenced Corrosion (MIC) of ground support. *Geotechnical and Geological Engineering* vol. 38, no. 1, pp. 375–387.

Epiroc. 2025. 'Vulcan Bolt' Online at https://www.epiroc.com/en-ba/products/rock-drilling-tools/ground-support/energy-absorbing-rockbolts/vulcan-bolt (accessed 13 January 2025).

Evans, D.W. 2022. Data cross validation for a newly commissioned dynamic drop test facility. The Australasian Institute of Mining and Metallurgy: Melbourne. pp. 320–328 .

Hadjigeorgiou, J., Dorion, J.F., Ghali, E. 2008. Support System Performance under Different Corrosion Conditions. *Journal of the Southern African Institute of Mining and Metallurgy* vol. 108, pp. 359–365.

Hadjigeorgiou, J., Savguira, Y., Thorpe, S.J. 2020. Impact of steel properties on the corrosion of expandable rock bolts. *Rock Mechanics and Rock Engineering* vol. 53, no.2, 705–721.

Hadjigeorgiou J., S.J. Thorpe and K.M. Cole 2023. Quality Assurance Considerations for Friction Rock Stabilizers. *Mining Technology (TIMM A).* vol. 132, no. 1, pp. 17–29.

Hadjigeorgiou, J., Thorpe, S.J., Storimans, E., Agrensa, F.D. 2024. Impact of steel properties on the susceptibility to corrosion of weld mesh and mesh straps. *The Journal of the Southern African Institute of Mining and Metallurgy* vol 124, no. 9, pp. 517–526.

Hayden, S.C., Chisholm, C., Eichmann, S.L., Grudt, R., Frankel, G.S., Hanna, B., Headrick, T., Jungjohann, K.L. 2022. Genesis of Nanogalvanic Corrosion Revealed in Pearlitic Steel. Nano Letters vol. 22, no. 17, pp. 7087–7093.

ISO 18265:2013. 2013. Metallic materials - Conversion of hardness values. Geneva: International Organization for Standardization (ISO).

Janik-Czachor, M., Szummer, A., Szklarska-Smialowska, Z. 1972. Effect of Sulphur and Manganese on Nucleation of Corrosion Pits in Iron. *British Corrosion Journal* vol. 7, no. 2, pp. 90–93.

Kadowaki, M., Muto, I., Takahashi, K., Doi, T., Masuda, H., Katayama, H., Kawano, K., Sugawara, Y., Hara, N. 2019. Anodic Polarization Characteristics and Electrochemical Properties of Fe3C in Chloride Solutions. *Journal of The Electrochemical Society* vol. 166, no, 12, C345–C351.

Knox & Hadjigeorgiou 2024a. Behaviour of Yielding Mechanical Hybrid Rockbolts under Complex Loading Conditions. International *Journal of Rock Mechanics and Mining Sciences* vol. 182.

Knox & Hadjigeorgiou 2024b. Direct impact load tests on mechanical hybrid rockbolts. *Australian Centre for Geomechanics: Montreal, Canada*. pp. 467–478.

Knox, G., Hadjigeorgiou, J. 2023. Performance in Shear of Mechanical Hybrid Rockbolts. Australian Centre for Geomechanics, Perth. pp. 495–506.

Sandvik. 2025. 'MD/MDX Bolt' Online at https://www.rocktechnology.sandvik/en/products/ground-support/bolts-and-cables/friction-bolts/md--mdx-bolt/ (accessed 13 January 2025).

Stern, M., Geary, A.L. 1957. Electrochemical polarization: a theoretical analysis of polarization curves. *Journal Electrochemical Society* vol. 104, no. 1, pp. 56–63.

Vallati, O., Darlington, B., Sandberg, L. 2022. Dynamic drop testing of Sandvik's D47 and D39 MDX bolts at the Swerim's testing facility. *The Australasian Institute of Mining and Metallurgy: Melbourne*. pp. 428–440. ◆